Network structure of turbulent premixed flames

Jasmeet Singh, Rahul Belur Vishwanath, Swetaprovo Chaudhuri, and R. I. Sujith

Citation: Chaos **27**, 043107 (2017); doi: 10.1063/1.4980135
View online: http://dx.doi.org/10.1063/1.4980135
View Table of Contents: http://aip.scitation.org/toc/cha/27/4
Published by the American Institute of Physics

Network structure of turbulent premixed flames

Jasmeet Singh,[1] Rahul Belur Vishwanath,[2] Swetaprovo Chaudhuri,[1,2,a)] and R. I. Sujith[3]
[1]*Department of Aerospace Engineering, Indian Institute of Science, Bangalore, India*
[2]*National Center for Combustion Research and Development, Indian Institute of Science, Bangalore, India*
[3]*Department of Aerospace Engineering, Indian Institute of Technology Madras, Chennai, India*

(Received 12 December 2016; accepted 3 April 2017; published online 13 April 2017)

In this paper, a generalized description of the complex topology of turbulent premixed flames stabilized in a model gas turbine combustor is obtained using network analysis. Networks are created using the visibility algorithm applied to points on the flame edge obtained from Hydroxyl radical (OH)—Planar Laser Induced Fluorescence images of turbulent premixed flames. The network structure thus obtained showed the emergence of a few massively connected nodes which were found to represent the folded regions of the flame front. These nodes, which are called the hubs of the network, are vital for determining the overall structure of the flame front. Degree distribution of the formulated networks is used to characterize the flame-turbulence interaction inherent in the system. Turbulent flame front networks were found to be rigid enough to be unaffected by random perturbations but highly vulnerable towards coordinated removal of hubs or folds. These findings could serve as the first network-analytic approach to characterize turbulence-flame interaction dynamics with the use of a flourishing network theory, which enhances ongoing works based on vortex dynamics, hydrodynamic stability, and thermo-acoustic instability. *Published by AIP Publishing*. [http://dx.doi.org/10.1063/1.4980135]

The network theory has been utilized in a diverse set of problems in the recent past. It has provided critical insights and modeling directions in systems as varied as the world wide web, disease spread to vortex dynamics in turbulent flows, and thermo-acoustic instability. These phenomena are highly non-linear and quite complex to study. In the present work, we use a network theoretic approach to study the topology of premixed turbulent flames, pervasive in modern propulsion engines or in a supernova Ia. Networks created from the flame fronts help us identify the critical regions on the flame, which appear to be the most vital for the constructed flame front networks. So far, probability density functions of single point descriptors, e.g., curvature, flame surface density function, or a global descriptor such as a fractal dimension of the entire flame contour could be found in the literature. However, these canonical local or global descriptors do not account for the mutual interaction between the neighboring flame elements. Instead, the network approach helps us study flame front dynamics as an aggregate of such interacting flame elements. The constructed networks appear to be resilient towards random perturbations but highly vulnerable to the removal of identified vital network nodes.

I. INTRODUCTION

The network theory has evolved in recent times to model real-world networks: artificial or natural, such as the internet and biochemical networks.[1–4] The application of the network theory has elucidated the dynamics of an epidemic spread[5] or an impending thermoacoustic instability in a combustor.[6] The analyses are based on the selection of network nodes and their mutual connectivity from available spatial or temporal data. Recently, an algorithm has been introduced to convert time series data into a network using the mutual visibility of peak data points as criteria.[7] This algorithm has been used widely to characterize and extract useful information from temporal data.[8–10] Similar to the network structure from time series data, parallel efforts have been made to convert spatial data into a network using the vorticity field of two-dimensional turbulence to understand its characteristics.[11] Network analysis has also been conducive to discriminating the various regions critical to the flow dynamics in turbulent heated jets.[12] These efforts have provided non-trivial insights into the system dynamics and can be possibly used to model or predict the investigated phenomenon.

Nair and Taira[13] have recently shown that the sparsification of networks formed from the vortical interactions does not change the spectral properties of these networks.[13] Such sparsification uses algorithms such as *Sparsify*[14] to produce spectrally similar sparse graphs. These sparse graphs have shown almost no change in the core vortex structures in vortex networks. These studies indicate that a few interesting points are sufficient to portray the overall dynamics of turbulent vortical interactions. The aforementioned works motivate the network analysis of a turbulent premixed flame surface topology presented in this paper. The analysis presented here could be readily applied onto any convoluted surface in turbulence, including but not limited to non-premixed flames, passive scalars, turbulent non-turbulent interfaces, and the surface of atomizing liquid jets.

Evolution of the flame front in a premixed turbulent flame is a complex process. Straining, folding of the flame surface by turbulence, and dilatation of the flow by the flame

a)Electronic mail: schaudhuri@aero.iisc.ernet.in

contribute to a highly convoluted, seemingly chaotic flame structure. Vortices ranging from the dimension of the order of the combustion chamber to the smallest Kolmogorov scales interact with the evolving flame front. These interactions render the multiscale system highly non-linear and quite complex to study. While most of the research studies in the field focus on the surface averaged properties of evolving surfaces[15–17] or the ensemble-averaged properties of flame locations evolving in time,[18–21] this work analyses the collective interaction of points embedded on the edge of the flame using the network theory. Subsequently, we will show that utilizing the insights obtained from the parameters of constructed networks, we were able to identify regions on the flame front, which are able to represent the overall physics and were key in representing the interaction between the flame front and turbulence.

II. EXPERIMENTAL METHOD

In the present study, a model gas turbine combustor consisting of three inline swirl burners has been utilized, the schematic of which is shown in Fig. 1. The air flow is supplied from a compressor through a series of pressure regulators and metered using a mass flow controller (ALICAT MCR, range: 0–4000 slpm) to obtain the desired mass flow rate. Fuel (Methane, 99% purity) is metered using a mass flow controller (ALICAT MCR, range: 0–500 slpm), which is then premixed with air in a mixing chamber. The mixture enters the settling chamber through 12 ports and flows through the ATG (Active turbulence grid) followed by a square convergent section and into the quartz test section where it is ignited. The ATG is designed for generating homogeneous turbulence based on the concepts of Makita,[22] Kang,[23] and Larssen.[24] The winglets in the ATG are placed in the horizontal position (plane of the burner) throughout this study. Three fixed vane angle (30°, 5 vaned) swirlers having an outer diameter (D) of 30 mm and a hub diameter of 10 mm are arranged linearly with an edge to edge spacing of 18 mm, which mimics a sector of an annular gas turbine combustor.

The turbulent cold flow was characterized using a single-probe hot wire anemometer at the centerline of the swirlers along the transverse direction to the flow. The mean and root-mean-square of the fluctuating component of velocities were obtained from the data measured at a sampling rate of 10 kHz for a time duration of 5 s. They are denoted by $\bar{U}$ and u'_{rms}, respectively. Figure 2 shows their profiles for different Reynolds Numbers (Re) obtained at a height of 2 mm above the swirler exit.

Planar Laser-Induced Fluorescence (PLIF) diagnostics was performed for the measurement of hydroxyl (OH) distributions within the premixed methane-air flame. The system is comprised of a Nd:YAG pump laser (Spectra-Physics Quanta-Ray *lab-Series* PRO-230, class IV single-pulsed) operating at 10 Hz and pumping a tunable dye laser (Sirah PrecisionScan PSCAN-G-30) containing Rhodamine 6 G. The generated laser beam at 567 nm is frequency doubled using a doubling crystal which emits a UV laser beam of wavelength 283.54 nm with a beam energy of about 20 mJ per pulse. The emitted UV beam is passed through cylindrical lenses and a collimator to produce a nearly parallel light sheet through the region of interest in the combustor test section. The fluorescence signal emitted by the excited OH radical is captured using an intensified relay optics (IRO) coupled CCD camera (LaVision Imager SX 4M). The light emitted due to fluorescence is captured using a UV lens and an enhanced OH filter having a transmission efficiency of ~75% with a central wavelength of 320 nm and a width of

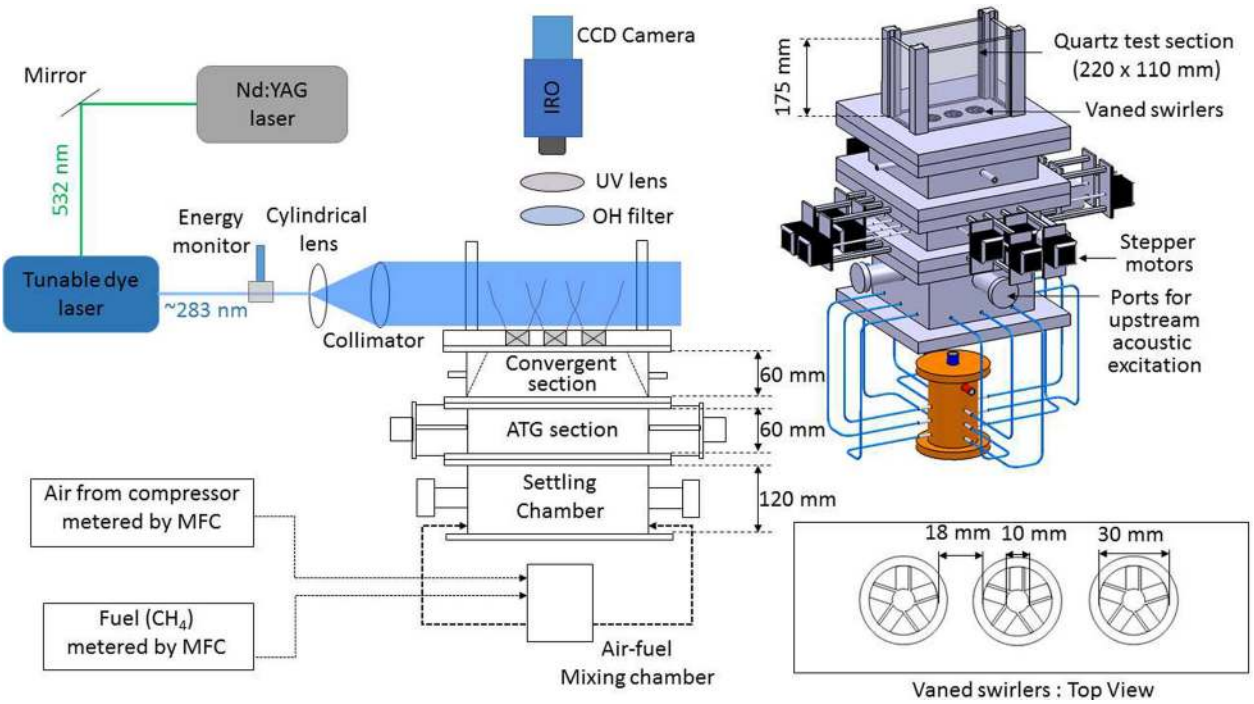

FIG. 1. Schematic of the experimental setup. ATG: Active Turbulence Grid.

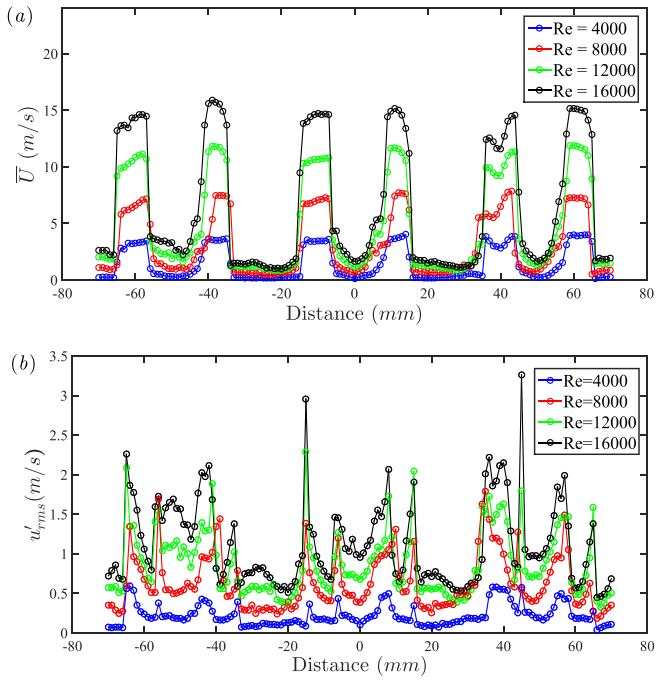

FIG. 2. (a) Mean velocity and (b) rms velocity profile obtained at the centerline of the swirlers along the transverse direction to the flow.

40 nm. The CCD camera was focused on a region of interest spanning 132 mm × 48 mm, which corresponds to a scale factor or resolution (Δ) of 0.165 mm/pixel.

Images were acquired for three values of the Reynolds number, i.e., 8000, 12 000, and 16 000. For all the three conditions, images were acquired for two values of equivalence ratios (ϕ), one near blowoff and the other far from blowoff. The ratios are presented in Table I.

The raw experimental images were corrected for laser sheet profiles and beam energy fluctuations from the pump laser. The quartz test section itself was used as a cuvette filled uniformly with acetone vapor for the laser sheet profile measurement. The fluorescence from the acetone vapor is captured with the same output beam energy but with the filter replaced. The filter used for acetone had a peak transmission efficiency of ∼70% at ∼405 nm, which falls within the emission spectra of acetone. The sheet correction involved averaging 100 individual images captured using the CCD camera. The energy fluctuations are corrected from the data stored using the energy monitor. Additionally, the scattered light from the background is subtracted from the images captured without the laser sheet. The corrected OH-PLIF images are used to extract the flame front locations. The flame front is considered to be the location of the maximum gradient in the OH concentration obtained from the flame images. The flame front extraction technique and subsequent network formulation are discussed in Section III.

TABLE I. Values of ϕ for near and far from blowoff cases.

Re	8000	12 000	16 000
Near blowoff	0.60	0.65	0.65
Far from blowoff	0.86	0.85	0.86

III. EXTRACTING NETWORK FROM PLIF DATA

A. Flame front from PLIF images

The images acquired from PLIF imaging are post-processed to identify the flame fronts from the flame stabilized at the central swirler. The original images are cropped to capture a physical area of 36.31 mm × 24.22 mm with an image dimension of 220 × 150 pixels as shown in Fig. 3(a). Although the flame fronts from the three swirlers interact at some distance from the swirler exit, the region of interest does not involve any such interaction between flames originating from different swirlers and captures only the flame stabilised at the central swirler. We identify the flame front using the Canny edge detection technique[25] which initially applies the non-maximum suppression to the intensity gradients of the image, then implements double thresholding to determine the potential edges, and finally tracks the edges by hysteresis to eliminate spurious edges. Reactant and product sides are identified using mean intensity values on either side of the flame front. These are marked in Figure 3(b) with symbols R and P denoting the reactant and product region, respectively. Network data will subsequently be extracted from the flame fronts identified through this process.

B. Flame front to the network

The extracted flame front corresponds to the iso-contour of the maximum gradient of the hydroxyl radical concentration. Multi-scale perturbations due to turbulence render the flame topology wrinkled and folded at multiple scales. Turbulent flow fluctuations may cause the flame fronts to entrap the reactant mass while in other instances, it may cause the flame segment to be detached from the main flame branch, thus creating a flame island. Therefore, the individual flame elements on a continuous or discontinuous front are always in close interaction with each other. Flame surfaces in turbulence are continuously generated by stretching and annihilated by folding and self-intersection processes over a range of length and time scales. A folded region of the flame, such as the one shown in Figure 4(a), gets detached from the flame front and forms a reactant island.[26] Subsequently, the reactants in this island would be consumed, and the flame surface in the erstwhile folded region will annihilate. This process leads to a major modification in the parent flame front structure. Carefully examining the figure, we can see that the flame positions which are the most susceptible to inducing such modifications have many other flame positions 'visible' from them. Hence, visibility serves as a combined measure for proximity and interaction between the flame elements. Conventional Eulerian studies of turbulent premixed flames generally study the pdf of flame properties say, for e.g., the curvature of the flame fronts. On the other hand, Langrangian studies are used to track points embedded on the flame front and then find the average properties over those points. In either of these domains of studies, it is difficult to identify the folded regions of the flame described above. Using network descriptors, we intend to highlight these high visibility regions of the flame.

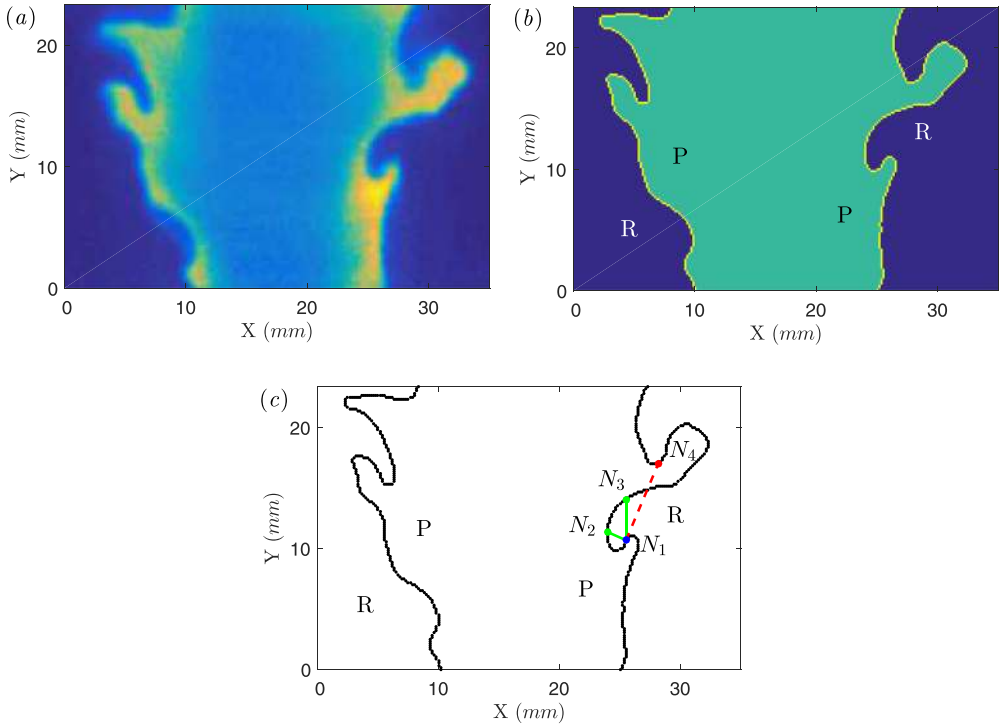

FIG. 3. Extracting the network from the PLIF image. (a) PLIF image depicting the spatial OH radical concentration variation. (b) Flame front identified from the PLIF image with reactant and product sides differentiated. (c) Illustration of the algorithm based on visibility to connect the nodes. The red dashed line means no connection while green lines mean that a connection exists between the respective nodes.

A complex system can be represented by more than one network, and the manner in which the complex network is constructed determines the characteristics of the complex system that is emphasized. Here, we want to emphasize visibility to highlight folds, and a network constructed on similar lines serves as a simple, yet revealing tool to analyze the phenomenon.

Efficient visibility algorithms have been formulated to convert temporal data into a network.[7,27] These algorithms take the visibility of the peaks of temporal fluctuations as the criteria to develop a network. The rationale behind this is that a data peak occurring at one instance will influence the data after it according to its own strength. A similar logic can be drawn while generating networks from spatial flame fronts. If there is a perturbation on a front, it will affect other parts of the flame depending upon the strength of the perturbation or the span of the region from where it can be witnessed. Hence, the visibility of one point from the other also

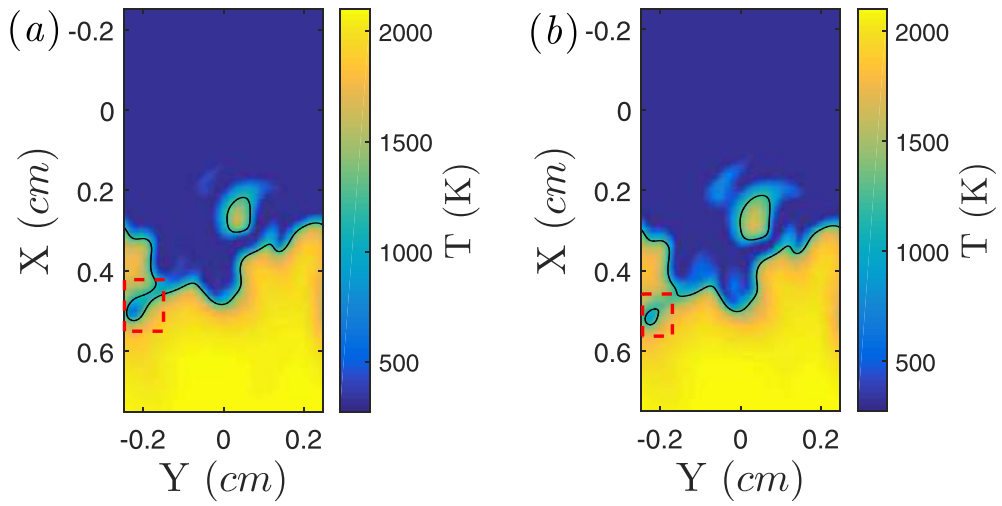

FIG. 4. Interaction between point positions defined in the convoluted region of the flame leading to modifications in the parent flame structure. (a) A branch of the flame front in which a reactant mass is about to detach itself from the parent flame. (b) The detached reactant island consumes the reactants and annihilates. Caused by the interactions of point positions defined on the flame front, the formation of such a reactant island modifies the parent flame front to a good extent. The images are volume slices of temperature (T) obtained from direct numerical simulations. Here, the flame front is identified using the iso-temperature contour corresponding to $T = 1190$ K. The square box highlights the detachment and annihilation of a reactant mass from the flame front. Reproduced with permission from Uranakara *et al.*, Combust. Flame **163**, 220–210 (2016). Copyright 2016 Elsevier.[26]

captures the influence of a perturbation at one point over the other.

A set of nodes N and the edges E between them uniquely define a graph or network $G(N, E)$.[3] We select the flame front positions as the nodes of the network. These are the points in the pixelated flame front image, which lie on the reaction front (eg., points N_1–N_4 in Figure 3(c)). Next, we go on to choose the edges of the network. An edge between two nodes indicates that they are in interaction with each other. We choose edges on the basis of visibility. Looking from the reactant side, if node N_i is 'visible' from node N_j, then they have an edge between them. The mutual visibility of nodes is defined as follows. Node N_i will be visible to node N_j if none of the pixels lying on the two-dimensional line of sight from N_i to N_j or vice versa represent the product side of the flame, i.e., all the pixels that best represent a hypothetical line joining the two nodes fall only on the reactant side or the flame front itself. The adjacency matrix of the formulated network is hence defined as

$$A_{i,j} = \begin{cases} 1, & \text{if } N_i \text{ is visible to } N_j, \\ 0, & \text{otherwise.} \end{cases} \quad (1)$$

Pixels which best represent the line-of-sight of N_i from N_j are found using the Bresenham algorithm.[28] This algorithm determines the points of an n-dimensional raster that should be selected in order to form a close approximation to a straight line between two points. A thresholding is used for the maximum length of connection between two nodes based on the concept of node similarity.[29] This states that any two of the nodes will be considered for connection only if the distance between them is less than a particular threshold value. We have chosen the threshold to be approximately equal to the integral length scale of flow to take into account all plausible connections between the nodes. The method discussed above uniquely identifies an unweighted network extracted from the flame front and will be consequently utilized to characterize it.

IV. RESULTS AND DISCUSSION

To analyze the topology of networks constructed from the stated algorithm, we calculate the degree (k_n) of the nodes ($i = 1, 2, 3, .., N$, where N is the total number of nodes) in the network. It is defined as

$$k_n = \sum_{i=1}^{N} A_{i,n}, \quad (2)$$

where k_n is the degree of the nth node. The probability that a node will have a degree k is denoted by $P(k)$. The variation of the parameter $P(k)$ with k is important to identify the dynamics of the system from the network topology.[30] It is to be noted that the image data are discrete and might not give a perfect representation of connections between adjacent pixels due to inaccuracies in the integer value arithmetic operations of the Bresenham algorithm for neighboring pixels. Hence, the nodes having a degree less than six are not considered in the further analysis of turbulent flame fronts.

A. Networks from known curves

The network structure of standard time series has been established in the literature. Pseudo-periodic time series correspond to random networks with a node degree following Gaussian distribution whereas chaotic time series generate networks that exhibit small world and scale-free features.[30,31] Also, a constant time series gives rise to a network with a single point degree distribution. For validating the algorithm developed here, we construct networks from artificially generated periodic sine-wave and straight line shaped flame front profiles. The pixel dimensions of the images containing these profiles were kept the same as those of the turbulent flame images. These artificial flame fronts serve as reference conditions for the more complex multi-scale turbulent flame fronts. Figure 5 shows these two conditions of the flame front along with their corresponding degree distributions plotted on a log-log scale. A straight line flame front gives rise to a network with all the nodes having the same degree. This is because all the nodes have the same visibility to all the other flame front nodes. On the other hand, a periodic sine-wave flame front generates a network with near-Gaussian degree distribution. Figure 5(d) shows the degree distribution scatter plot of such a sine-wave curve. A curve fitted to these data is also shown with a dashed line. To show a comparison with a network having degrees distributed according to Gaussian probability, we construct such a network with the same number of nodes as the sine-wave profile network. Nodes in this network have degrees distributed according to the Gaussian distribution with the same mean value as the mean of degree distribution of the sine-wave profile. The degree distribution of such a network is also plotted in Figure 5(d). The networks are constructed for the same number of nodes, and degree distribution is plotted

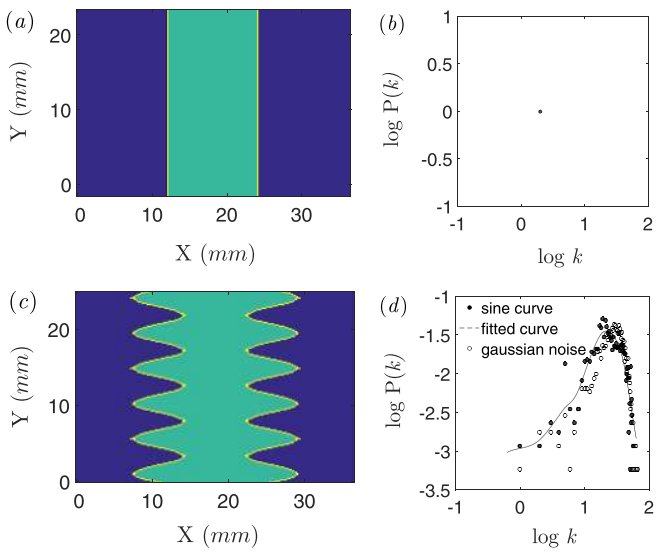

FIG. 5. (a) Flame as a straight line. (b) Corresponding degree distribution comes out to be a single point as all the nodes have the same degree. (c) Flame as a sine-wave. (d) Corresponding degree distribution along with a network having Gaussian degree distribution.

with identical bin sizes for the two networks. The two degree distributions show a significant overlap. This is because the degrees are randomly distributed about a given value in the case of a periodic curve flame front. Most of the nodes on the flame front will have a degree value approximately equal to the mean of the distribution while a few of the nodes occurring on the crests and the troughs of the front will have a high and low value of degree, respectively. This reflects that the periodic flame front cycles or perturbations are uncorrelated with one another. Thus, a straight line flame front would produce a constant degree distribution, and a periodic flame front profile such as a sine-wave would result in a random graph when processed using the aforementioned algorithm.

B. Network structure of turbulent premixed flames

We proceed to construct networks from the flame front profiles obtained from the PLIF images. Unweighted networks are constructed from images acquired for all six experiment conditions using the procedure described in Sec. III B. The degree distribution of the networks constructed from flame fronts at $Re = 8000$ and $\phi = 0.60$ averaged over 80 flame images is plotted in Figure 6(a). The color of the scatter plot changes from red to yellow as the degree of the nodes increases. In contrast to the near-Gaussian degree distribution showed by a periodic sine-wave curve, the turbulent flame front profile gives rise to a network with highly heterogeneous distribution of degrees. Most of the nodes of this network have low degree values, exhibited by high P(k) for low k. These nodes appear as red and black nodes in the degree distribution. Only a few nodes have a very high degree value. They appear as orange or yellow in the degree distribution. These massively connected nodes or so-called hubs emerge in the network constructed from the turbulent premixed flame. This gives rise to a right-skewed degree distribution.

Investigating further to find the location of the hubs emerging in the network over the PLIF images, we color the flame front positions or nodes in the images according to the degree they correspond to. Such representative images are shown in Figures 6(b)–6(d). Interestingly, the nodes which are having a higher degree represent the folds occurring on the flame front. It is possible that in convoluted regions such as these, turbulent vortices compete with the flame front to align it according to its vortical structures.[32,33]

The emergence of hubs in the networks constructed from the acquired images could be attributed to the turbulence-flame interaction in the corresponding folded regions of the flame. These folded regions lead to self-intersection towards reactant island formation and eventually flame surface annihilation[26,34] to eventually cause large fluctuations in the turbulent flame speed, i.e., the averaged propagation rate of the entire flame. Also, recent studies show that these folded regions are characterized by a very high local displacement flame speed.[18,26] These regions of the flame are represented by parts of the flame front folded towards the product side, which are significantly modified by the presence of turbulence. Hence, a strong influence of turbulence over selected regions of the flame forces these folded regions to appear as

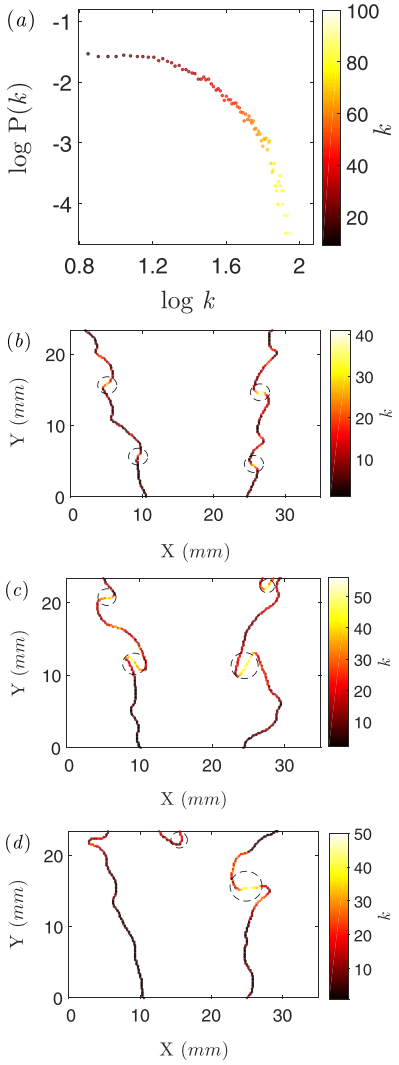

FIG. 6. (a) Scatter plot of the degree distribution networks constructed from flame fronts at $Re = 8000$ and $\phi = 0.60$ averaged over 80 flame images. The color of the scatter plot changes with the degree of the nodes. (b)–(d) Representative flame images colored with respect to the degree of the nodes. Clusters of high degree nodes which denote the folded regions of the flame front that are marked with dashed circles.

the most significant ones in the network. This contributes to the highly right-skewed degree distribution of the network.

Visualization of a network helps in determining its structure. To explicitly differentiate between the structure of networks emerging from various profiles of the flame front studied here, we use the graph visualization software *Gephi*[35] to visualize them. The visualized networks are shown in Figure 7. The size and the color of the nodes of the network are decided by the degree they carry. Smaller nodes in the network have lower degree values while larger ones have a higher degree. Also, the color of the nodes changes from green to red as we go from lower to higher degree values. For a straight line flame front profile, we witness a uniform degree distribution as shown in Figure 7(b). All the nodes have the same degree and thus have the same size and color. The network structure formed from a sine-wave profile is shown in Figure 7(d). The degree distribution of such a flame front was near-Gaussian. This is corroborated by the visualization as

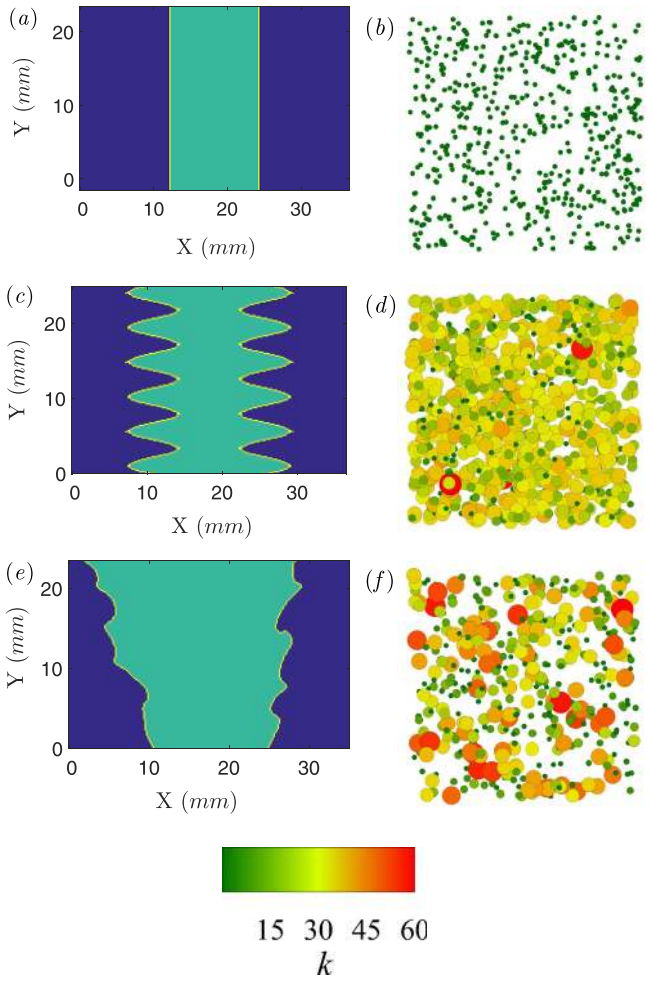

FIG. 7. Pseudo-flame front images of a (a) straight line and (c) periodic sine curve. The corresponding network structure is shown in (b) and (d), respectively. The size of the nodes shown is set by the degree they carry. Higher degree nodes are larger than the nodes with a lower degree. Also, the color of the nodes changes from green to red with an increase in the degree. (b) Uniform network structure is seen in the case of a straight line flame front. (d) Random network structure of the sine-wave flame front with most of the nodes having a mean value of degree. (e) Turbulent flame front profile from the experiment. (f) Network structure of the corresponding turbulent flame front profile showing most of the nodes as lower degree green nodes while only a few appear as highly connected red ones.

most of the network nodes appear mid-sized with few large or small sized nodes.

Figure 7(e) shows a turbulent flame front profile, and Figure 7(f) shows the corresponding network. Most of the nodes in the network are small sized green colored nodes. These nodes carry smaller degree values. Only a few nodes are large sized red nodes. These are denoted as the hubs of the network. As we can see, a clear distinction between the network structure emerging from constant, periodic, and turbulent flame front profiles is made through the presented visualization. Network hubs emerging in the turbulent flame network are distinctively seen. It has been established from Figure 6 that these hubs are folded regions of the flame front primarily concave towards the reactants' side of the mixture.

To convey the significance of the hubs of the networks constructed from turbulent flames, we use a network parameter $l_{network}$ called the characteristic network length or the average short path length. It is defined as

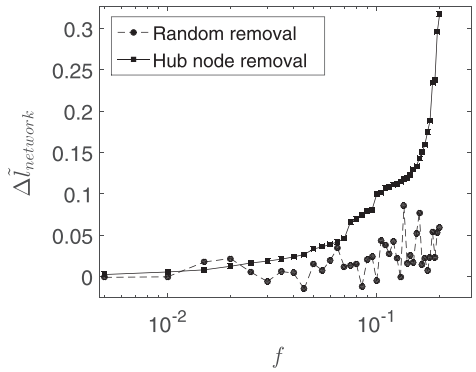

FIG. 8. Changes in the normalized characteristic network length $\Delta\tilde{l}_{network}$ of a turbulent flame front network for random node and hub node removals. (a) Near blowoff, (b) far from blowoff, and (c) degree distribution.

$$l_{network} = \frac{1}{N(N-1)} \sum_{i \neq j} d(i,j), \tag{3}$$

where $d(i, j)$ is the shortest path length between node N_i and node N_j. This distance is based on the network adjacency matrix and not the physical distance between the flame front nodes. We calculate $d(i, j)$ using Dijkstra's shortest path algorithm.[36] To measure the change in flame front interaction caused by a disturbance in the network, we can consider how the removal of flame front nodes modifies the characteristic network length.

The changes in the flame network characteristic length $l_{network}$ as a result of the removal of network nodes in a random manner and in a systematized fashion selectively eliminating the hub nodes are outlined in Figure 8. The systematic hub node removal is done starting from the highest degree node downwards. We plot the changes in the normalized characteristic network length

$$\tilde{l}_{network} = \frac{l_{network}(f) - l_{network}(f=0)}{l_{network}(f=0)} \tag{4}$$

for various fractions of node removal f for one of the flame front networks (flame shown in Figure 3). The flame front network is resilient towards random perturbations which occur majorly in the low curvature regions of the flame. This is apparent from the characteristic network length being unaffected even for a large fraction f of nodes being removed. However, the removal of hubs occurring on the folds greatly modifies the flame network, which is visible from the substantial change in the network length. A small value of the average path length, such as in our case, indicates that nodes are linked through a very short path. However, if we remove hub nodes, i.e., the nodes from the folded regions of the flame, the average path length increases dramatically. This suggests that, on the flame, there will be a sudden drop in the probability of interaction between any two nodes selected at random, and the network average path length increases sharply. Hence, even small changes to the folded structures on the flame front provide a very effective way to modify the complete flame dynamics.

As seen from the resilience study of the turbulent flame network, the removal of hub nodes from the network or the

folded regions of the flame results in a substantial increase in the average path length of the network, while the removal of network nodes at random does not change the average path length much. This kind of behavior would not hold for an unperturbed laminar flame. We can consider the previously discussed pseudo-straight line flame front as an unperturbed laminar flame. Such a flame is non-convoluted and does not undergo turbulence-flame interactions. In the network created from such a flame front, the nodes have the same degree value. Hence, the removal of nodes in any fashion will not change the average path length in such a network.

Networks were constructed for all six experimental conditions given in Table I. The degree distribution obtained from these conditions averaged over 80 flame front image networks is plotted in Figure 9. The distributions for the same Reynolds number are plotted together. As the flame front is turbulent, in all these conditions, we get a similar degree distribution profile for all the conditions. However, there is a slight shift in the distribution towards higher probability for higher degree nodes as we move from far from the blowoff equivalence ratio to the near blowoff one. The statistical similarity of the near and far-from blowoff cases for the three Reynolds number was checked using the Kolmogorov-Smirnoff test.[37] The asymptotic p-value of the test was found to be 0.99, 0.57, and 0.03 for the case of $Re = 8000$, $Re = 12\,000$, and $Re = 16\,000$, respectively. p is the probability of observing a test statistic as extreme as, or more extreme than, the observed value under the null hypothesis that the two cumulative distribution functions are from the same continuous distribution. Hence, the shift is significant only for the case of $Re = 16\,000$ (see Figure 9(i)).

The instantaneous flame front in turbulent premixed combustion is highly convoluted, and the position of reaction zones moves rapidly in space. This produces a range of areas in a two-dimensional space representing the possible flame front positions. Figure 10 shows the superposition of instantaneous reaction fronts at near and far from blowoff conditions for the case of $Re = 8000$ and $Re = 16\,000$. The apparently thick zone created by overlapping fluctuating flame edges, seen in this figure, is referred to as the turbulent flame brush. As we move from a higher equivalence ratio to a lower one, we approach blowoff. This leads to broadening of the flame brush and causes the degree distribution to shift

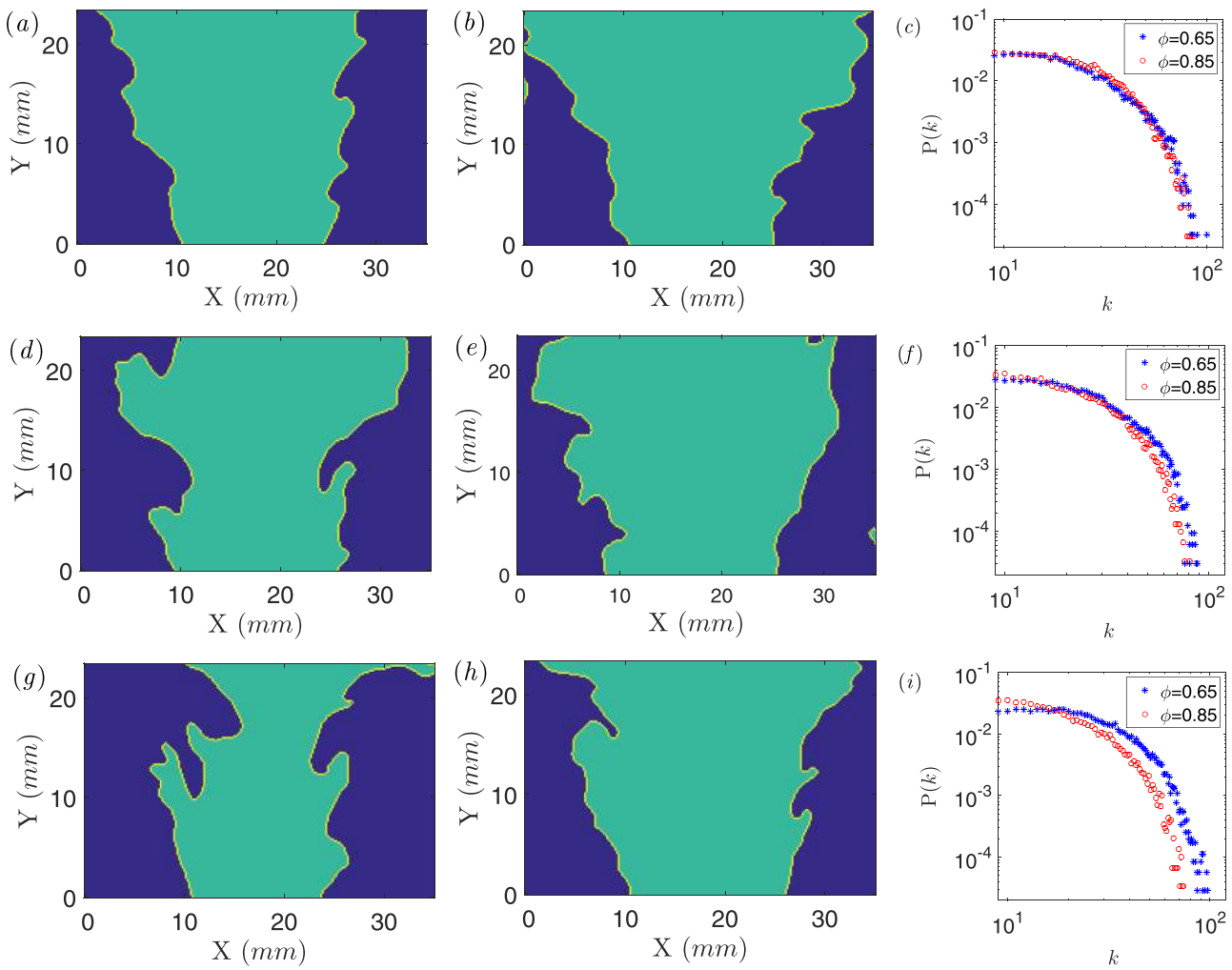

FIG. 9. Representative flame front images are shown for the $Re = 8000$ case at (a) near and (b) far from blowoff conditions. Scatter plot of the degree distribution averaged over 80 images for both the conditions is given in (c). Similarly, (d)–(f) and (g)–(i) correspond to $Re = 12\,000$ and $Re = 16\,000$, respectively. With a shift in ϕ, i.e., the equivalence ratio from far from blowoff to near blowoff, a slight shift of the distribution towards higher P(k) for larger k values is seen for the higher Reynolds number cases. (a) Near blowoff and (b) far from blowoff.

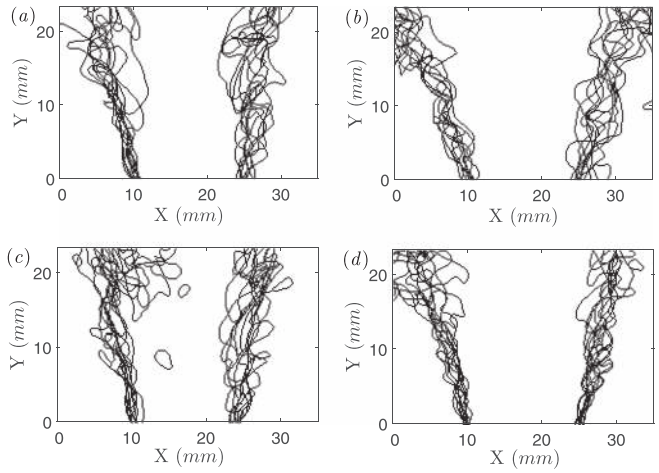

FIG. 10. Superposition of instantaneous reaction fronts for $Re = 8000$ ((a) and (b)) and $Re = 16\,000$ ((c) and (d)).

towards higher k values. The highly distorted flame front structure near blowoff has been observed using PLIF imaging in the literature,[38,39] but here we have quantified the same using network analysis. This phenomenon is explained in greater detail in the next paragraph.

For the cases of lower equivalence ratios, the flames are closer to the leaner blowoff limit and are more susceptible to flow disturbances.[40] This increases the flame brush thickness for flames near blowoff conditions.[41–44] On the other hand, flames with a higher equivalence ratio, which are far from blowoff, tend to be more stable and are less susceptible to local turbulent eddies. This leads to a thinner flame brush. This increase in the flame brush thickness with decreasing ϕ is reflected in the increase in the probability of higher degree network nodes as we go from the far from blowoff to near blowoff condition. This shift can also be interpreted as follows. As the flame brush thickness increases when we move from higher to lower ϕ, there is a higher probability of finding the flame front over a wider range of coordinates, or simply, the two-dimensional flame front spans through a wider area. Folds on the flame front extend deeper into the product side of the front. This further increases the visibility of the nodes on the folds of the flame making their degree even higher. Thus, the degree distribution shifts towards higher k for the hubs of the network as we go from the far from blowoff to near blowoff case.

The shift in the degree distribution is perceived distinctly only in the $Re = 16\,000$ case and is not substantial for the lower Reynolds number cases ($Re = 8000$ and $Re = 12\,000$). This is probably due to the better flame stability, lower lean blowoff limits, and near laminar flamelet behavior for the case of lower Re.[40] As such, the flame regime shifts gradually from the flamelet regime at $Re = 8000$, $\phi = 0.86$ to the thin-reaction zone regime at $Re = 16\,000$, $\phi = 0.65$. These regimes can be identified using the Karlovitz number, Ka, which is the ratio of the turbulence time scales to the chemical time scales. The regime shifts from the laminar flamelet regime to the thin-reaction zone regime as we increase the Karlovitz number (tabulated in Table II (Appendix)).

The flamelet regime occurs when the relevant chemical time scale is short compared to the convection and diffusion time scales. In this regime, combustion takes place within the asymptotically thin layers embedded in the turbulent flow. These layers, which have a well-defined inner structure, are called flamelets.[45] In the flamelet regime, both the preheat and reaction zones are thinner than the smallest turbulent eddies. Hence, though curved or stretched, the flamelet retains the basic structure of a laminar flame. On the other hand, for flames lying in the thin-reaction-zone regime, the reaction zone still retains its laminar structure, whereas the preheat zones are perturbed and thickened by small-scale turbulent eddies, with temperature fluctuations observed therein.[46] With this shift, the smallest turbulence scales start to enter and modify the transport within the reactive states. Small eddies that enter the preheat zone broaden the flame alongside, increasing the width of the flame brush. Hence, the degree distribution is shifted towards higher k values for the near blowoff case (higher Ka) at higher turbulent intensity conditions ($Re = 12\,000$ and $Re = 16\,000$).

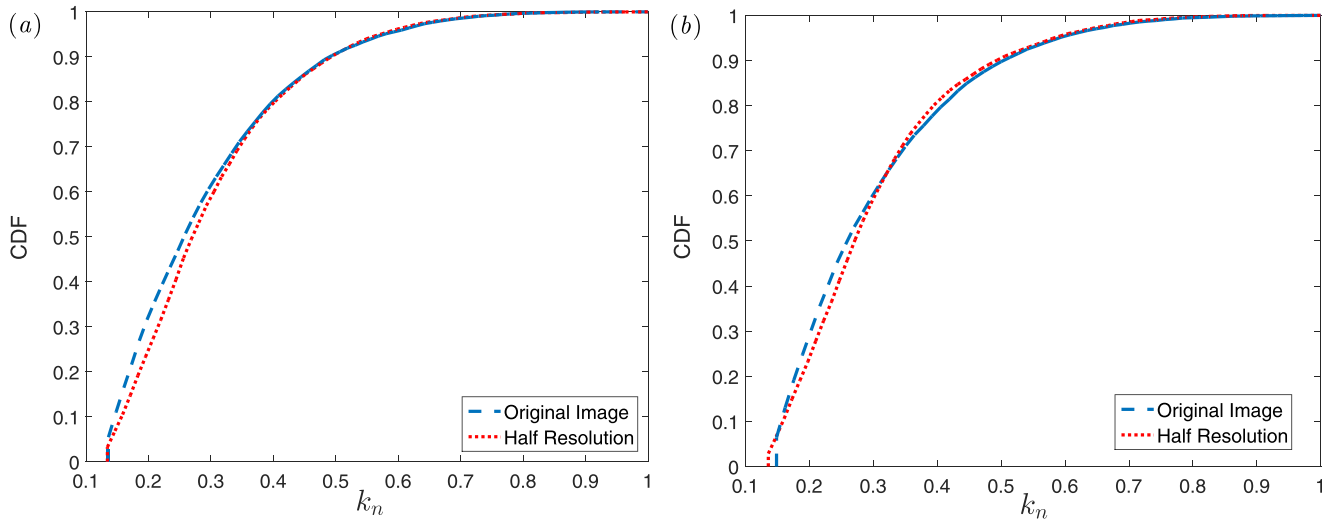

FIG. 11. Cumulative distribution function is plotted for the original PLIF images, and the images coarsened to half of the original resolution for two conditions (a) Re = 12 000 and (b) Re = 16 000, both far from blowoff. Here, the degree values are normalized (k_n) with the maximum degree of the respective network.

It is worth mentioning that the resolution of the PLIF images considered in the present study is 0.165 mm/pixel, whereas the flame thickness, which can be considered as a measure of the smallest length scale for flame perturbation, is much bigger. 1 pixel from the image is not more than 2.54 times the Kolmogorov length scale (refer Table II). Typically, DNS is done at a similar spatial resolution. Thus, the images are well resolved for the present study. Additionally, to check for the robustness of the present study, the analysis was repeated for resized images with resolution (Δ) as low as half the resolution of the original acquired images. The number of nodes, which were in the range of 30 000–35 000, decreased to about one third, i.e., in the range of 10 000–12 000. The two-sample Kolmogorov-Smirnoff statistic test was conducted on degree values of the nodes obtained from the two images to check whether the fine and the coarse images resulted in similar probability distribution. The asymptotic p-value for all the six conditions was found to be well over the significance level of 0.05. The null hypothesis is considered untrue if the value of p is less than a significance level (usually taken as 0.05). Hence, the distributions are not statistically dissimilar even after decreasing the image resolution to half the original value. The comparison of the cumulative distribution functions of two such conditions is shown in Figure 11. As we make the images coarser, the distributions diverge. The p-value for the Kolmogorov-Smirnoff test decreases to a lower value. If we decrease the resolution further, the number of nodes (data points) considered would be insufficient to conduct a statistical test such as a Kolmogorov-Smirnoff test. Hence, images whose resolution is far less than half the resolution of the original images, i.e., far less than 110×75 pixels, would not give the desired results. However, as seen from the figure, the distributions do not become statistically dissimilar even for a 50% reduction in the resolution.

V. CONCLUDING COMMENTS

To the authors' knowledge, this work is a first effort to characterize a turbulent flame front using network analysis. An algorithm is introduced to convert convoluted flame contours into networks on the basis of visibility. Pseudo-flame front images from known curves were created to establish the validity of the algorithm. The straight line and periodic sine-wave flame front gave rise to uniform and random networks, respectively. The network structure thus obtained matches very well with the ones constructed from constant and pseudo-periodic time series.[30]

Networks were constructed using the developed algorithm for turbulent flame fronts from images acquired using PLIF imaging on a model gas turbine combustor. These networks had highly right-skewed degree distribution with hubs emerging on the network. The hubs were found to exist in the large curvature folded regions of the flame front. Turbulent eddies distort the flame at these locations and create folded structures on the flame front, thus increasing the visibility of these regions. Hence, the strong influence of turbulence on these selected regions of the flame makes them appear as the hubs of the network. These networks were found to be resilient against random perturbations (random node removal) while they were quite susceptible to the removal of nodes representing folds (hub nodes).

A shift in the degree distribution was witnessed as we move from the far from blowoff to near blowoff case for higher turbulent intensity. This shift is attributed to the thickening of the flame brush as we approach blowoff because the flame front becomes unstable and more susceptible to modifications from turbulent eddies.

Understanding the dynamics of the flame front in the collective using network analysis gives a new viewpoint of gaining insight into turbulent combustion. Instead of computing field properties over a set of points and then calculating an average to understand the behavior of the system, this method utilizes interactions inherent in the system to characterize it. Conventional studies, from either the Eulerian or Lagrangian point of view, presently do not make use of such insights. Analyzing the flame front using simple mathematical tools from the network theory has provided us with essential control points of the flame front, which are highlighted by the degree distributions of the constructed networks. Recent studies have suggested methods that identify the most sensitive points in the network which opens up the possibility for control.[47–49] Controlling each and every flame front in turbulent combustion is probably impractical. However, network analysis of the phenomenon provides us with the key points on the flame front that are most influenced by turbulence. Hence, network theory based analysis is a simple, yet revealing alternative to study the turbulent flames.

ACKNOWLEDGMENTS

The support of Department of Science and Technology, India, sponsored National Center for Combustion Research and Development, IISc is gratefully acknowledged.

APPENDIX: FLAME FLOW PROPERTIES AND CONVERGENCE OF $P(K)$

1. Turbulent flame properties

The bulk flow velocity of the reactants through the swirlers is calculated as

$$U_{bulk} = \frac{Q}{A}, \tag{A1}$$

where Q is the volume flow rate of reactants through the mass flow controller, and A is the effective area of the cross-section of the swirlers. Re, which is the ratio of inertial forces to viscous forces is calculated as

TABLE II. Turbulent flame properties.

Re	ϕ	Re_t	Ka	$u'_{rms}(m/s)$	δ_L (mm)	S_L (cm/s)	η (mm)	Δ (mm/px)
8000	0.60	237	3.96	0.63	1.11	11.14	0.0992	0.165
	0.86	236	0.86	0.63	0.52	32.14	0.0994	0.165
12000	0.65	328	4.01	0.88	0.87	15.23	0.0777	0.165
	0.85	328	1.45	0.88	0.53	31.46	0.0778	0.165
16000	0.65	419	5.79	1.12	0.87	15.23	0.0647	0.165
	0.86	419	2.02	1.12	0.52	32.14	0.0648	0.165

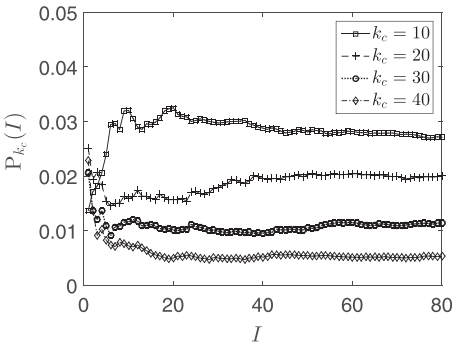

FIG. 12. Plot of $P_{k_c}(I)$ with I.

$$Re = \frac{U_{bulk} D}{\nu}, \tag{A2}$$

where D is the outer diameter of the swirler, and ν is the kinematic viscosity of air. The turbulent Reynolds number, Re_t, is calculated as

$$Re_t = \frac{\langle u'_{rms} \rangle L}{\nu}, \tag{A3}$$

where $\langle u'_{rms} \rangle$ is the mean of the rms of the fluctuating component of velocity recorded using a hot wire anemometer over the length of the combustor (see Figure 2(b)), L is the integral length scale taken as $D/5$, and ν is the kinematic viscosity of air. We calculate the length scales of smallest turbulent eddies η using[50]

$$\eta \approx \frac{L}{Re_t^{3/4}}. \tag{A4}$$

Finally, we compare the time scales of turbulence with those of chemical reactions using the Karlovitz number, Ka (Ref. 50)

$$Ka \approx \left(\frac{\delta_L}{\eta}\right)^2, \tag{A5}$$

where δ_L is the laminar flame thickness calculated using CHEMKIN with the GRI 3.0 mechanism.[51] All the calculated parameters are provided in Table II.

2. Convergence of P(k)

A convergence study was done to check for the convergence of P(k) values with the number of images processed. The value of P(k) for a specified number of images I and a constant value of degree k_c is denoted as $P_{k_c}(I)$. We plot $P_{k_c}(I)$ versus I for the case of $Re = 8000$, $\phi = 0.60$ in Figure 12. The plot starts to converge at 20 images and finally converges at around 60 images. We get similar convergence results for all the six cases examined.

[1]R. Albert and A.-L. Barabási, "Statistical mechanics of complex networks," Rev. Mod. Phys. **74**, 47–97 (2002).
[2]M. E. Newman, "The structure and function of complex networks," SIAM Rev. **45**, 167–256 (2003).
[3]M. Newman, *Networks: An Introduction* (Oxford University Press, 2010).
[4]A. Barrat, M. Barthelemy, R. Pastor-Satorras, and A. Vespignani, "The architecture of complex weighted networks," Proc. Natl. Acad. Sci. U. S. A. **101**, 3747–3752 (2004).
[5]M. Barthélemy, A. Barrat, R. Pastor-Satorras, and A. Vespignani, "Velocity and hierarchical spread of epidemic outbreaks in scale-free networks," Phys. Rev. Lett. **92**, 178701 (2004).
[6]M. Murugesan and R. Sujith, "Combustion noise is scale-free: transition from scale-free to order at the onset of thermoacoustic instability," J. Fluid Mech. **772**, 225–245 (2015).
[7]L. Lacasa, B. Luque, F. Ballesteros, J. Luque, and J. C. Nuno, "From time series to complex networks: The visibility graph," Proc. Natl. Acad. Sci. **105**, 4972–4975 (2008).
[8]X. Xu, J. Zhang, and M. Small, "Superfamily phenomena and motifs of networks induced from time series," Proc. Natl. Acad. Sci. **105**, 19601–19605 (2008).
[9]R. Friedrich, J. Peinke, M. Sahimi, and M. R. R. Tabar, "Approaching complexity by stochastic methods: From biological systems to turbulence," Phys. Rep. **506**, 87–162 (2011).
[10]R. V. Donner, Y. Zou, J. F. Donges, N. Marwan, and J. Kurths, "Recurrence networks—A novel paradigm for nonlinear time series analysis," New J. Phys. **12**, 033025 (2010).
[11]K. Taira, A. G. Nair, and S. L. Brunton, "Network structure of two-dimensional decaying isotropic turbulence," J. Fluid Mech. **795**, R2 (2016).
[12]A. Charakopoulos, T. Karakasidis, P. Papanicolaou, and A. Liakopoulos, "The application of complex network time series analysis in turbulent heated jets," Chaos **24**, 024408 (2014).
[13]A. G. Nair and K. Taira, "Network-theoretic approach to sparsified discrete vortex dynamics," J. Fluid Mech. **768**, 549–571 (2015).
[14]D. A. Spielman and N. Srivastava, "Graph sparsification by effective resistances," SIAM J. Comput. **40**, 1913–1926 (2011).
[15]J. H. Chen and H. G. Im, "Correlation of flame speed with stretch in turbulent premixed methane/air flames," in *Symposium (International) on Combustion* (Elsevier, 1998), Vol. 27, pp. 819–826.
[16]J. H. Chen, E. R. Hawkes, R. Sankaran, S. D. Mason, and H. G. Im, "Direct numerical simulation of ignition front propagation in a constant volume with temperature inhomogeneities. I. Fundamental analysis and diagnostics," Combust. Flame **145**, 128–144 (2006).
[17]H. G. Im and J. H. Chen, "Effects of flow strain on triple flame propagation," Combust. Flame **126**, 1384–1392 (2001).
[18]S. Chaudhuri, "Life of flame particles embedded in premixed flames interacting with near isotropic turbulence," Proc. Combust. Inst. **35**, 1305–1312 (2015).
[19]S. Pope, "Lagrangian pdf methods for turbulent flows," Annu. Rev. Fluid Mech. **26**, 23–63 (1994).
[20]P. Yeung and S. Pope, "Lagrangian statistics from direct numerical simulations of isotropic turbulence," J. Fluid Mech. **207**, 531–586 (1989).
[21]S. Girimaji and S. Pope, "Propagating surfaces in isotropic turbulence," J. Fluid Mech. **234**, 247–277 (1992).
[22]H. Makita and K. Sassa, "Active turbulence generation in a laboratory wind tunnel," in *Advances in Turbulence 3: Proceedings of the Third European Turbulence Conference Stockholm, July 3–6, 1990*, edited by A. V. Johansson and P. H. Alfredsson (Springer, Berlin/Heidelberg, 1991), pp. 497–505.
[23]H. S. Kang, S. Chester, and C. Meneveau, "Decaying turbulence in an active-grid-generated flow and comparisons with large-eddy simulation," J. Fluid Mech. **480**, 129–160 (2003).
[24]J. V. Larssen and W. J. Devenport, "On the generation of large-scale homogeneous turbulence," Exp. Fluids **50**, 1207–1223 (2011).
[25]J. Canny, "A computational approach to edge detection," IEEE Trans. Pattern Anal. Mach. Intell. **PAMI-8**, 679–698 (1986).
[26]H. A. Uranakara, S. Chaudhuri, H. L. Dave, P. G. Arias, and H. G. Im, "A flame particle tracking analysis of turbulence–chemistry interaction in hydrogen–air premixed flames," Combust. Flame **163**, 220–240 (2016).
[27]B. Luque, L. Lacasa, F. Ballesteros, and J. Luque, "Horizontal visibility graphs: Exact results for random time series," Phys. Rev. E **80**, 046103 (2009).
[28]J. E. Bresenham, "Algorithm for computer control of a digital plotter," IBM Syst. J. **4**, 25–30 (1965).
[29]M. Scholz, "Node similarity as a basic principle behind connectivity in complex networks," J. Data Mining Dig. Human. (published online, 2015).
[30]J. Zhang and M. Small, "Complex network from pseudoperiodic time series: Topology versus dynamics," Phys. Rev. Lett. **96**, 238701 (2006).

[31]J. Zhang, J. Sun, X. Luo, K. Zhang, T. Nakamura, and M. Small, "Characterizing pseudoperiodic time series through the complex network approach," Phys. D: Nonlinear Phenom. **237**, 2856–2865 (2008).
[32]N. Chakraborty, M. Klein, and N. Swaminathan, "Effects of Lewis number on the reactive scalar gradient alignment with local strain rate in turbulent premixed flames," Proc. Combust. Inst. **32**, 1409–1417 (2009).
[33]P. E. Hamlington, A. Y. Poludnenko, and E. S. Oran, "Interactions between turbulence and flames in premixed reacting flows," Phys. Fluids **23**, 125111 (2011).
[34]J. H. Chen, T. Echekki, and W. Kollmann, "The mechanism of two-dimensional pocket formation in lean premixed methane-air flames with implications to turbulent combustion," Combust. Flame **116**, 15–48 (1999).
[35]M. Bastian, S. Heymann, and M. Jacomy, *Gephi: An Open Source Software for Exploring and Manipulating Networks* (International AAAI Conference on Weblogs and Social Media, 2009).
[36]E. W. Dijkstra, "A note on two problems in connexion with graphs," Numer. Math. **1**, 269–271 (1959).
[37]F. J. Massey, Jr., "The kolmogorov-smirnov test for goodness of fit," J. Am. Stat. Assoc. **46**, 68–78 (1951).
[38]S. Chaudhuri, S. Kostka, M. W. Renfro, and B. M. Cetegen, "Blowoff dynamics of bluff body stabilized turbulent premixed flames," Combust. Flame **157**, 790–802 (2010).
[39]S. Chaudhuri, S. Kostka, M. W. Renfro, and B. M. Cetegen, "Blowoff mechanism of harmonically forced bluff body stabilized turbulent premixed flames," Combust. Flame **159**, 638–640 (2012).
[40]P. Griebel, E. Boschek, and P. Jansohn, "Lean blowout limits and nox emissions of turbulent, lean premixed, hydrogen-enriched methane/air flames at high pressure," J. Eng. Gas Turbines and Power **129**, 404–410 (2007).
[41]V. Karpov and E. Severin, "Turbulent burn-up rates of propane-air flames determined in a bomb with agitators," Combust., Explos. Shock Waves **14**, 158–163 (1978).
[42]I. Shepherd, "Flame surface density and burning rate in premixed turbulent flames," in *Symposium (International) on Combustion* (Elsevier, 1996), Vol. 26, pp. 373–379.
[43]M. Wu, S. Kwon, J. Driscoll, and G. Faeth, "Turbulent premixed hydrogen/air flames at high reynolds numbers," Combust. Sci. Technol. **73**, 327–350 (1990).
[44]P. Griebel, R. Bombach, A. Inauen, R. Scharen, S. Schenker, and P. Siewert, "Flame characteristics and turbulent flame speeds of turbulent, high-pressure, lean premixed methane/air flames," in *ASME Turbo Expo 2005: Power for Land, Sea, and Air* (American Society of Mechanical Engineers, 2005), pp. 405–413.
[45]N. Peters, "Laminar flamelet concepts in turbulent combustion," in *Symposium (International) on Combustion* (Elsevier, 1988), Vol. 21, pp. 1231–1250.
[46]A. Lipatnikov, *Fundamentals of Premixed Turbulent Combustion* (CRC Press, Boca Raton, Florida, 2012).
[47]X. F. Wang and G. Chen, "Synchronization in small-world dynamical networks," Int. J. Bifurcation and Chaos **12**, 187–192 (2002).
[48]W. Yu, G. Chen, and J. Lü, "On pinning synchronization of complex dynamical networks," Automatica **45**, 429–435 (2009).
[49]P. DeLellis, M. di Bernardo, and M. Porfiri, "Pinning control of complex networks via edge snapping," Chaos **21**, 033119 (2011).
[50]C. K. Law, *Combustion Physics* (Cambridge University Press, Cambridge, England, 2010).
[51]R. J. Kee, F. M. Rupley, and J. A. Miller, "Chemkin-ii: A fortran chemical kinetics package for the analysis of gas-phase chemical kinetics," Technical Report (Sandia National Labs., Livermore, CA, USA, 1989).